World Conference on Timber Engineering Oslo 2023

STRUCTURAL CHARACTERISTICS AND DEFORMATION BEHAVIOUR OF AN ADVANCED CARPENTRY CONNECTION IN TIMBER CONSTRUCTION

Katrin Vögele[1], Moritz Tronnier[2], Yannick Plüss[3], Mike Sieder[4]

ABSTRACT: The following paper addresses the experimental examination of the micro-offset-node, used in an innovative roof structure "ReFlexRoof" developed in the public funded project TimberPlan+ (research consortium led by HTWK Leipzig, Team FLEX). The structural form of the micro-offset-node, called MVK, leads back to a carpentry connection by Friedrich Zollinger. The characteristics of the MVK are described in more detail. In order to represent the load-bearing and deformation behaviour of the roof structure realistic input values for the nodal stiffness in the existing three-dimensional design model are needed. Therefore, laboratory tests on the micro-offset-node are executed at the Institute of Building Construction and Timber Structures (iBHolz, Technische Universität Braunschweig). The experimental methodology as well as observations during the experiments are presented. Based on load-deformation curves, resulting values for the strength and stiffness of the node are calculated. Apart from that, the methodical and manufacturing procedure is examined and discussed.

KEYWORDS: carpentry connections, glued laminated timber, connection stiffness, experimental results

1 INTRODUCTION

Carpenter connections are not part of the static and engineering calculation methods commonly used today. They usually form hyperstatic spatial trusses or frames and are mainly found in historical constructions. Due to the traditional origin of these connections and the associated lack of knowledge about realistic stiffness values of such timber connections, it is difficult for civil engineers to determine the load-bearing capacity and the deformation behaviour of these structures. [1] Today's building codes do not provide sufficient calculation methods to evaluate the connection stiffness and determine the values for numerical or analytical calculations. Therefore, such constructions are calculated on the basis of statically determined simplified models.
However, this approach no longer fits the state of the art. For numerical computational methods and simulations, the nodal stiffness values of these structures are required in order to calculate the internal force distribution. An estimation of the stiffness is not sufficient for hyperstatic structures with multiple nodes. Incorrect and unrealistic assumptions can lead to underestimation of the internal forces and, in the worst case to structural failure.
Regarding the micro-offset-node as an advanced carpentry connection and the ReFlexRoof as a hyperstatic structure, this problem became apparent in the research studies of the TimberPlan+ project.

2 STRUCTURAL DESIGN

The micro-offset-node, described in the following as MVK (German translation "**M**ikro**v**ersatz**k**noten"), is an advanced carpentry connection in the timber roof structure called ReFlexRoof. The structure of the roof can be described as a lamella roof and is shaped as an arch.

2.1 ORIGIN

The first evidence of lamella roofs can be found in the middle of the 16th century. Philibert de l'Orme had cut planks into arch shapes, joined them with wooden nails and wedged them lengthwise. [2] Friedrich Zollinger adopted this construction method in 1921 and formed the planks into a rhombic construction of lamellae instead of a layered connection [3], as shown in Figure 1.

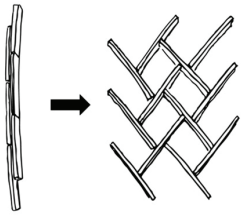

Figure 1: *Adaption of the structure from l'Orme (left) to Zollinger (right) [4]*

This formation of the lamellae generates a reciprocal framework.

[1] Katrin Vögele, iBHolz Technische Universität Braunschweig, German, k.voegele@tu-braunschweig.de
[2] Moritz Tronnier, iBHolz Technische Universität Braunschweig, German, m.tronnier@tu-braunschweig.de
[3] Yannick Plüss, iBHolz Technische Universität Braunschweig, Germany, y.pluess@tu-braunschweig.de
[4] Mike Sieder, iBHolz Technische Universität Braunschweig, Germany, m.sieder@tu-braunschweig.de

https://doi.org/10.52202/069179-0199

Nodes of the Zollinger structure are characterized by a continuous lamella, to which another lamella is butted from both sides. The connection of the node and thus the lamellae is ensured by a bolt that is guided through an oblong shaped hole in the continuous lamella. On the upper side, the lamellae are curved due to the arch shape of the roof construction. On the bottom side the lamellae are straight.
For the completion of the roof boarding planks are attached which are assumed to figure as secondary structure. [3] Zollinger patented this system in 1923. [5]
Although the advantages in the standardization of components formed a fundamental prerequisite for economic efficiency, the weak points of this system became apparent over the years: The ductility of the connection due to the difference in materiality of timber and steel and the arrangement of the bolt generate forces transverse and at an angle to the fibre. This leads to local deformations at the node. In the global structure, these deformations are amplified in association with the redundancy and the creep of timber under external load. All these interactions lead to settling of the structure and thus to change of the internal load distribution. This effect amplifies as the spans become longer. For this reason, the MVK (Figure 2) was developed, which offers the following advantages: [6]

- Precise joinery methods
- Use of kiln-dried timber
- Use of form-fit principle without a bolt

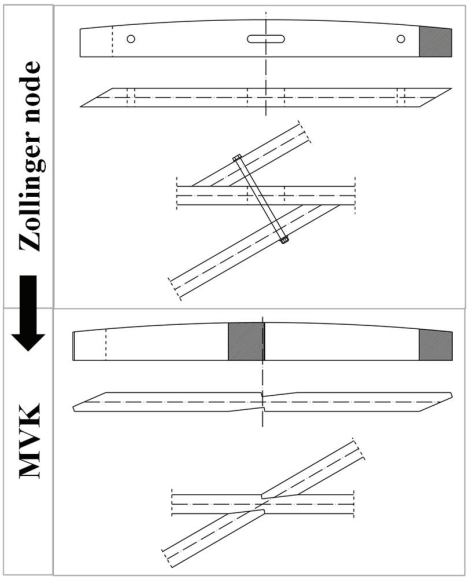

Figure 2: *Illustration of the Zollinger node in comparison to the MVK*

2.2 CURRENT LOCAL AND GLOBAL STRUCTURE

As described, the MVK is an attempt to optimise the traditional Zollinger joint and aims to reduce the creep deformations that can be observed in the construction.
The MVK consists of a step joint with two-sided incision shown in Figure 2. This ensures that the normal forces are transmitted via contact pressure. [6] In contrary to the construction of Zollinger the lamellae are not attached or connected to each other using fasteners. Similar to the original approach is that the lamellae are spanned in a rhombic shape which creates a framework of reciprocal even modules.

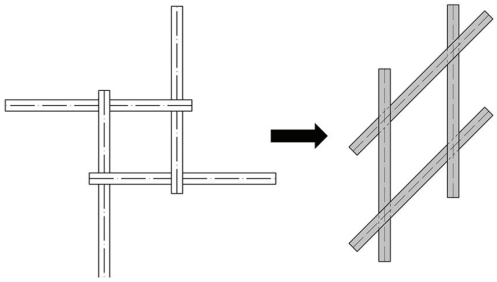

Figure 3: *An example of a reciprocal framework (left) that can be converted into a rhombic shape module (right)*

Several of these reciprocal modules then build an arch shaped roof. The construction is bordered by planks at the gable and by an edge beam the eaves as shown below.

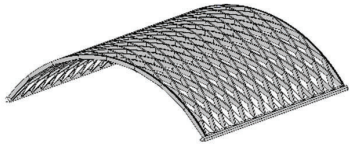

Figure 4: *Construction of the arch shaped roof*

To form the roof structure and to ensure the global load-bearing behaviour, the construction of the lamellae is sheathed with a panel. The connection between the panel and the lamellae is made by staples.
In the global view, the structure forms a highly hyperstatic system due to the great number of reciprocal modules. The consequence is, that the stiffness values of the nodes are highly important for the structural design.
In addition, the construction of the arch shaped roof is segmented. Several MVK-connected lamellae are bonded via a standardized panel element in the factory and are transported to the construction site. At the site the elements are combined to form the final structure.
During building of the prototype construction in the research project, it is discovered that the segments could not always be joined properly. This results in gaps between the lamellae at the node points (Figure 5, right).

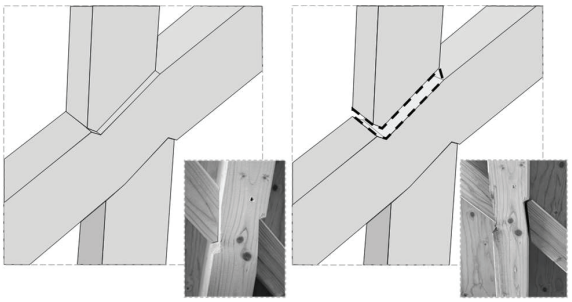

Figure 5: *Local node properties in the quasi-perfect (left) state and in the pre-deformed state (right)*

https://doi.org/10.52202/069179-0199

On one hand, these occur due to material and manufacturing inaccuracies, which are significantly more demanding to implement on the construction site because of the spatial geometry and assembly. On the other hand, the pre-curved planking causes recoil forces, which lead to pre-deformations.
In the research project these aspects have to be examined more closely.

3 MATERIAL AND METHODS

Although the basic local characteristics are approximately known from tests on preliminary models of the MVK [6], the MVK itself and its local load-bearing and deformation behaviour has not yet been extensively examined. Particularly the stiffness of the node has to be evaluated in more detail.

3.1 EXPERIMENTAL INVESTIGATION

With the aim to provide stiffness properties for the use in a computation design model, experimental investigations are carried out at iBHolz.

3.1.1 SETUP

All test specimens are made of two half-lamellae, which are butted on a continuous lamella. The loads are restricted to a compressive force acting axially on the upper lamella. This based on the assumption of an arched roof structure, which follows the line of thrust in the most optimal form. The geometric properties are selected based on the prototype. In order to contain the estimated load within the maximal capacity of the testing machine, the geometric dimensions of the prototype are scaled to the following dimensions:

$$h_S = 14\ cm \qquad t_v = 1.33\ cm$$
$$h_D = 12\ cm \qquad \gamma = 49.5°$$
$$b_D = b_S = 8\ cm$$

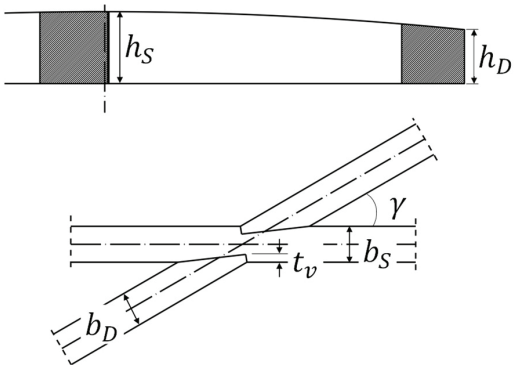

Figure 6: *Definition of the geometric variables at the lamella (top) and at the node (bottom)*

All lamellae are made of GL24h graded glulam timber. The average density of the timber used in the specimens is about 450 kg/m³.
The test concept consists of three test series with five test specimens each. The test series differs as shown in Table 1:

Table 1: *Description and over-view of the test series*

Series	Panel	Screws	Gap
A	x	-	-
B	x	-	x
C	-	x	-
***C4 / C5**	-	-	-

*the screws were removed after an applied load of 5 kN

The panel has a stapled connection (1.53x50 mm) to the lamellae. The spacing of the staples is 120 mm. 12 mm pine multiplex plywood is used as panel. The connection is ensured by three (6x120 mm) screws per half lamella. These are inserted as suggested in the patent for the MVK. In series B, a gap of 1 cm to the front-notch surface and 1 cm to the bottom-notch surface is created as shown in Figure 5 (on the right).

The tests are conducted on a walter+bai LFM 125 testing machine with a maximum capacity of 125 kN. The machine force as well as the displacement of the top pressure plate are recorded. The specimens are tested between two pressure plates which are connected to the testing machine via hinges. This assures that no bending moments are introduced by the compression plates. Before the load is applied the specimens have to be held in place by a supporting frame. The test frame is made of aluminium as shown below.

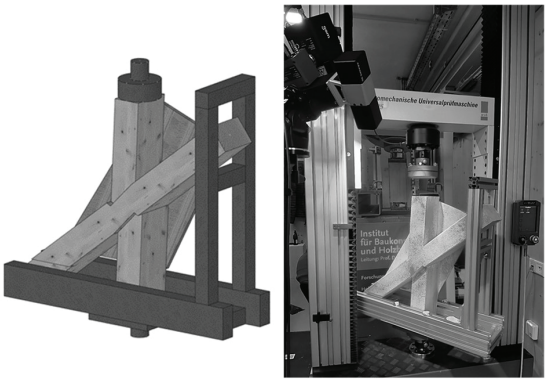

Figure 7: *Model of the test setup (left) and realization (right)*

It is ensured that no forces are transferred from the specimens to the testing frame during the experiment. The tests are accompanied by a photogrammetric measuring system, which takes 200 to 800 pictures per specimen and can be recalled at any time. In addition to the data from the testing machine this system allows further investigation of the load bearing behaviour of the node. The strain at the surface of the timber members can be measured and visualized by the software. The system replaces otherwise used strain gauges. In order to track the deformations, the specimens are painted white with a random black pattern to create better contrast for the measurements.

https://doi.org/10.52202/069179-0199

3.1.2 EXECUTION

The specimens are conditioned at 20°C and at a relative humidity of 65 % prior to the experiments. The average moisture content during the experiments is 11.5 %.
The tests are performed along the lines of DIN 26891. A preload is applied to clamp the specimen between the pressure plates before the hinges are untightened and the rotation of the pressure plates is made possible. A stress-controlled hysteresis cycle is performed between 40 % and 10 % of the expected maximum load. This eliminates any slip and ensures good contact between the lamellae. During the second cycle, the load is increased up to 60 % of the estimated load before switching to deformation control at 0.05 mm/s.
The experiments are terminated when the specimen fails and the load decreases rapidly or when the free movement of the specimen is limited by the testing frame. This happens at different piston displacement values for any specimen and is therefore monitored manually. In most cases the latter condition occurs first, due to the highly ductile behavior of the connection.

3.2 ANALYSIS

Currently, the computational model consists of a combination of beam and shell elements designed as a spatial frame model. The beam elements represent the lamellae and the panels are implemented as shell elements. For simple joints it is sufficient to consider the connection either as rigid or hinged. For more complex timber structures, the nodal stiffness needs to be characterized to provide a realistic internal force distribution.
The experimental investigation is designed to obtain stiffness values in axial direction of the lamella. Based on the load-deformation curves, an axial node stiffness C_x for the beam element (illustrated in Figure 8) can be determined.

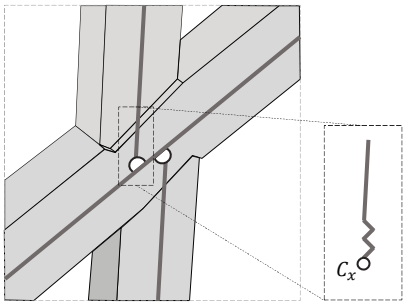

Figure 8: *Extraction of the lamella into a beam element with the node stiffness* $\boldsymbol{C_x}$ *at the joint to the continuous lamella*

Due to the pre-deformed conditions on the node, the specification of the node stiffness must include not only the stiffness in the quasi-perfect state but also the pre-deformed state (Figure 5). These two states represent the two static limit values for the stiffness of the structure.

Therefore, two methods are adopted to evaluate the characteristic mean stiffness C_x in the limit states:

- Heimeshoff and Köhler method (= HaK) [8]
- DIN EN 26891:1991 (= DIN) [9]

For the evaluation of the stiffness, the longitudinal deformation in direction of fibre of the lamella is neglected. The reason for choosing this method is that the longitudinal deformation compared to the total measured displacement does not exceed 2.5 %. The determination of the node stiffness is then simplified to half of the measured displacement regardless for both methods. In addition, for each test series only the measured values of the deformation from the second ascending branch of the hysteresis is taken into account. This excludes the initial slip. In test series B, which has significantly more slip due to the gap, the mean value of the measured slip of the setup from A and C ($u_{slip,set}$) is subtracted in order to be able to represent the effect of the gap at maximum load.

The following description summarizes the approach for the HaK and DIN method. Each load-deformation curve is analysed using both methods.

HaK method (compare to Figure 9):

1) Determination of the 95% fractile of the strengths for $f_{c,\alpha}$ and f_v according to [11] and [12]
2) Estimation of the expected loads $R_{dim,i}$ (equations based on the EC5/NA verifications for carpenter connections [13], [14])

$$R_{dim,compression} = t_v \cdot h_D \cdot \frac{f_{c,\alpha}}{\cos^2 \frac{\gamma}{2}} \tag{1}$$

$$R_{dim,shear} = 8 \cdot t_v \cdot k_{cr} \cdot h_S \cdot \frac{f_v}{\cos \gamma} \tag{2}$$

3) Formation of the mean value $R_{dim,mean}$ from the two proofs (shear force, contact pressure) of EC5/NA
4) Determination of the deformation $u_{R,dim}$ at the load $R_{dim,mean}$
5) Composition of the node stiffness C_x

$$C_x = \frac{R_{dim,mean}}{u_{R,dim}} \tag{3}$$

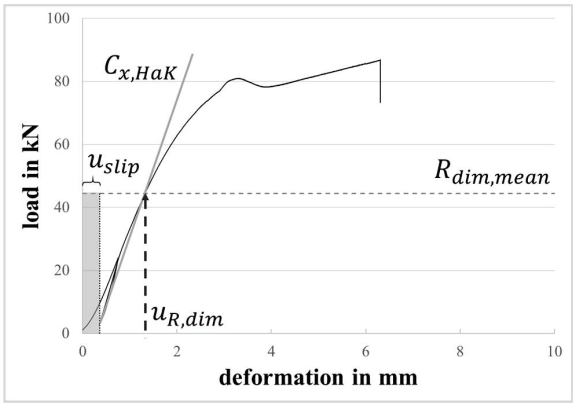

Figure 9: *Illustration of the approach based on the HaK method*

https://doi.org/10.52202/069179-0199

DIN method (compare to Figure 10):

1) Definition of the assumed elastic limit $R_{max,el}$
2) Determination of deformations u based on $0.4\ R_{max,el}$ and $0.1\ R_{max,el}$
3) Composition of the node stiffness C_x

$$C_x = \frac{0.4\ R_{max,el} - 0.1\ R_{max,el}}{u_{0.4\ R_{max,el}} - u_{0.1\ R_{max,el}}} \quad (4)$$

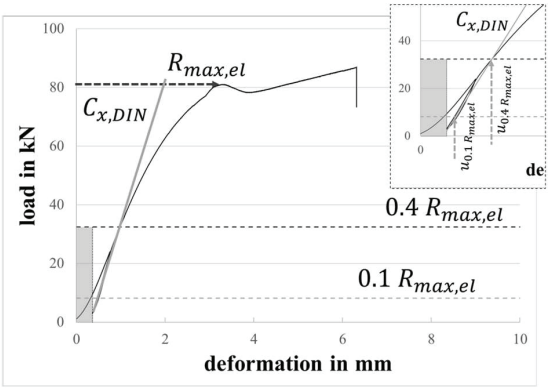

Figure 10: *Illustration of the approach based on the DIN method*

For the evaluation of test series B, a few minor adjustments are made. For the HaK method, the load-bearing capacity of the staple connection is considered to determine $R_{dim,mean}$. The determination of the initial deformation $u_{R,dim}$, the $u_{slip,set}$ is subtracted.

In the DIN method, a slightly different procedure is chosen in step 3. In equation (4), the stiffness is calculated with the consideration of u_{gap} following equation (5) and Figure 11:

$$C_x = \frac{0.4\ R_{max,el} - 0.1\ R_{max,el}}{(u_{0.4\ R_{max,el}} - u_{0.1\ R_{max,el}}) + \frac{3}{4} \cdot u_{gap}} \quad (5)$$

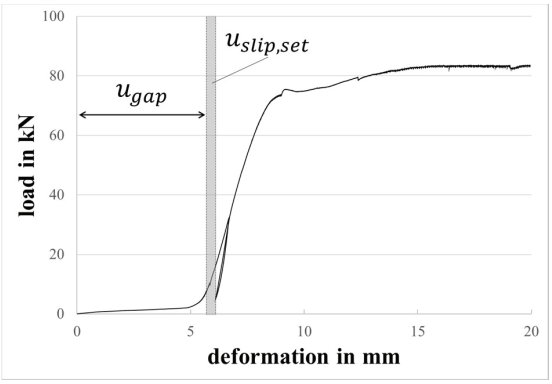

Figure 11: *Representation for the different deformations from the gap and the slip of the setup on one of the test specimen B*

The calculation of the characteristic values of the load-bearing capacity and stiffness is performed according to DIN EN 14358 Section 3 [14]. For the load-bearing capacity, a normal distribution is assumed according to $R_{c,90}$ in [11]. For the stiffness, the characterized mean value is calculated using the given equation 14 in [14].

4 RESULTS

The obtained node stiffness can be used in the numerical model to perform a sensitivity analysis for the evaluation of the internal force distribution. The following results are averages based on an evaluation of all test specimen.

4.1 ELASTIC LOAD-BEARING CAPACITY

For the value of the load-bearing capacity, the first maximum point of the load-deformation is used to determine the elastic limit $R_{max,el}$. To characterize this value to a 5%-quantile, [14] states a factor for a sample size of 5 specimens with

$$k_s(5) = 2.46$$

for the standard deviation.

The calculated standard deviation is applied to the mean values leading to the following characteristic load-bearing capacities $F_{k,el}$:

Table 2: *Average and characteristic values for the load-bearing capacity in the elastic limit state with sample size 5*

Test Series	$R_{max,el,mean}$ [kN]	s_y [-]	$F_{k,el}$ [kN]
A	73.3	7.045	56.0
B	68.1	6.101	53.1
C	66.1	8.384	45.5

It can be seen that the panel has an influence on the load-bearing properties of the node. Thus, A and B show up to 15% to 20% greater values than C at the characteristic value. The screws (in series C) that hold the step joint in position have only little influence on the elastic load-bearing capacity. By excluding C4 and C5 (MVK under preload without screws) from the evaluation of test series C, the values both of the mean and characteristic value differ by less than 4 %. However, it can be clearly noticed that the tests in C have a lower load-bearing capacity than A and B. It is assumed that the panel has a load-bearing effect, which is missing in test series C. In addition to that, the panel prevents the middle lamella from rotating and therefore loosing of form-fit.

The nodes in the overall structure are a combination of the cases A through C, A and B are randomly distributed whereas case C only occurs in planned matter. Therefore, the evaluation can be conducted over a larger sample size. The factor for the sample size decreases with the number of specimens. For the node states A, B the factor is

$$k_s(10) = 2.10$$

and for the node states A, B, C the factor is reduced to

$$k_s(15) = 1.99.$$

This allows to calculate the characteristic load-bearing capacity $F_{k,el}$ according to the Table 3.

Table 3: *Average and characteristic values for the load-bearing capacity in the elastic limit state with sample size 10 or 15*

Test	$R_{max,el,mean}$	s_y	$F_{k,el}$
Series	**[kN]**	**[-]**	**[kN]**
A, B, C	69.2	8.264	52.7
A, B	70.7	6.927	56.5

The difference in the load-bearing capacity of the node is about 7% larger for a composed case of A and B in comparison to the composed case A, B and C.
In order to compare the values with the state of art, the load-bearing capacity is determined according to the equations (1) and (2) which are derived from EC5 NDP [10]. The input strength properties are based on the 5%-fractile and on the 95%-fractile on EC5 [15]. The strength properties from NDP [10] are not used, because k_{cr} which reduces the width in order to limit the shear strength to an admissible value of 2.5 N/mm². $F_{dim,shear}$ would therefore be equal on the characteristic and on the 95 %-fractile level.
The evaluated values are shown in the following table.

Table 4: *5 %-fractile and 95 %-fractile for the load-bearing capacity according to [10] and [15]*

	$F_{5\%,DIN}$	$F_{95\%,DIN}$
	[kN]	**[kN]**
$F_{dim,compression}$	26.4	42.4
$F_{dim,shear}$	53.8	120.9

The characteristic result values of the experiments are close to the 5 %-fractile of $F_{dim,shear}$ as well as in the range of the 95 %-fractile of $F_{dim,compression}$. This shows that higher compressive forces can be transmitted via the step joint of the MVK than assumed by the design model in [10].

4.2 NODE STIFFNESS

Based on the presented methods in section 3.2 the following results for the axial stiffness C_x can be made as shown in the table below. For the analysis another evaluation is performed in test series B. It is listed as B' and shows the stiffness that results after the closure of the gap. The pre-deformation up to the point of contact in the step-joint is on average 5.27 mm based on measurements within the load deformation curve.

Table 5: *Average values for the node stiffness in the elastic limit state with sample size 5*

Test	$C_{x,DIN}$	$C_{x,HaK}$	u_{slip}
Series	**[N/mm]**	**[N/mm]**	**[mm]**
A	53453	49027	0.39
B	4682	5718	0.40*
B'	45608	53580	0.40*
C	48977	45972	0.41

*$u_{slip} = u_{slip,set}$; mean value out of u_{slip} from A and C

Comparing the two methods in each test series, differences in percentages can be observed: For A and C the differences are rather small and less than 10 %. For test series B, the percentage value increases up to 18 %. In case of the additional study B' the deviations are up to 15 %. A comparison of all lines (with exception of B) show, that the stiffnesses for a quasi-perfect node range from 45 kN/mm up to 53 kN/mm.
Considering Table 6, showing the composed test series, it is noticeable that the methods are converging and deviating by a maximum of 3,5 %.

Table 6: *Average values for the node stiffness in the elastic limit state with sample size 10 or 15*

Test	$C_{x,DIN}$	$C_{x,HaK}$
Series	**[N/mm]**	**[N/mm]**
A, B', C	49346	49526
A, B'	49531	51304

4.3 GENERAL OBSERVATIONS

Most of the deformation can be observed at the front-notch and bottom-notch surface (Figure 12) of the MVK.

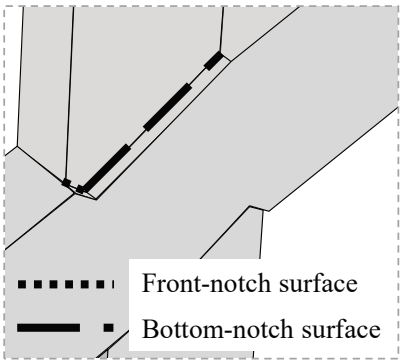

Figure 12: *Illustration of the position of the two surfaces*

At the beginning of the load application, the deformation shifts from the top lamella towards the front-notch surface. With further displacement, the bottom-notch surface is also compressed. As a result, a gap opens at the bottom-notch surface and remains as plastic deformation (Figure 13). Furthermore, it can be identified that the fibres of the abutting lamella protrude beyond the front surface. In addition, the abutting lamella rotates clockwise. Due to the compression on the front, the lamella tends to lose its optimal position. Thus, it is pushed out of the front-notch surface. This leads to an eccentricity of the resulting force and the lamella rotates. This rotation occurs especially in the test series B. Presumably, this is due to the lack of rotational support of the staple connection beyond its elastic limit. The displacement between the panel and the lamellae remains a plastic deformation after unloading.

https://doi.org/10.52202/069179-0199

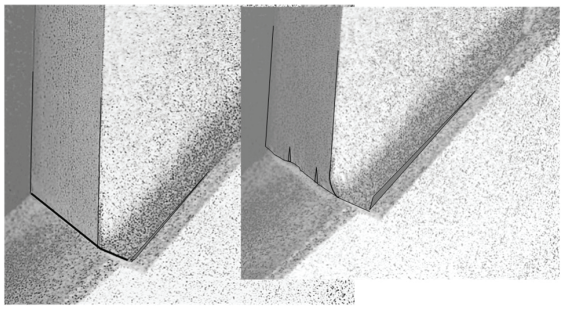

Figure 13:*Illustration of the deformations during the test phase (left) and after the test phase (right), which shows the permanent plastic deformation*

Furthermore, in test series B it is observed that the gap does not always close optimally. This means that a force- and form-fit connection cannot be guaranteed. These effects that occur at the quasi-perfect MVK are intensified in test series B. The tests in series C do not show a significantly different behaviour. In test C4 and C5 the screws are removed after applying a preload. This results in a complete failure by the abutting lamella popping out of the connection at the front-notch.
In general, the failure state of the MVK is determined by the deformations at the front-notch. The stresses in the bottom-notch surface are not decisive for the MVK.

4.4 APPROACH FOR DESIGN

For the determination of internal forces with FE-models, a limit value consideration for the stiffness for specific node states should be attempted. Therefore, three methods can be generated:

1) Design in the ultimate limit state
Historical research [16] shows that it can be assumed that the gaps are closing over time.
As long as it is ensured that the staples and quasi-perfect MVK provide enough plastic deformations capacity to close gaps, the stiffness for determining forces in the lamellae can be considered as the stiffness determined in series A and B':

$$C_x = 49000\ N/mm$$

2) Robustness estimation
In case of insufficient plastic deformation capacity of the quasi-perfect MVKs in an area next to a concentration of pre-deformed MVKs the risk of brittle failure must be addressed. An estimation for the robustness allows to find areas in the structure with a higher risk of failure due to load redistribution from softer node points. Therefore, two stiffness values have to be defined for the numerical model. The lower limit should be applied to nodes within the structure with open gaps.

- **Upper limit for quasi-perfect nodes** (test series A):
$$C_x = 53000\ N/mm$$
- **Lower limit for pre-deformed nodes** (test series B):
$$C_x = 4600\ N/mm$$

If it is considered to use screws to ensure the form-fit of the MVK, variant C can be adapted to the methods shown above.

5 DISCUSSION

Since there is no agreement in the literature ([8], [16], [17], [18], [19]) on how to evaluate the stiffness on carpenter-type connections in modern constructions, the following provides some views on the methodology, results and optimisation.

5.1 ANALYSIS METHOD

For the analysis up to the elastic limit state the linear elastic material law is observed and applied for further calculations.

Hysteresis effect is left out of the evaluation, since the MVK with gap is used to examine the effects of slip in the connection. In addition, the quasi-perfect MVK is manufactured with an accurate fit. For the investigation of the effects of repeated loads applied after closing of the gaps, cyclic tests shall be carried out.

In test series B (pre-deformed node), the nodal stiffness is very low if the closure of the gap is included in the determination of the linear elastic section. The method as proposed by HaK assumes this. The method proposed by DIN excludes this effect by default, as the stiffness value for the linear-elastic section is determined between 10 % and 40 % of the maximum load. The HaK method is therefore modified in B', and the DIN method in B in order to compare the stiffness values obtained in both methods.

If the stiffness is set as a gradient in comparison to the load-deformation curve, two areas between load-deformation curve and gradient are created (Figure 14): In the first one, the load-deformation curve is lower than the gradient. This leads to an overestimation of the internal load in the connected members and the node. In the second area there is an underestimation, because the gap of the MVK is closed. For the ultimate limit state, the overestimation of the stiffness is on the safe side, whereas an underestimation of the stiffness is on the unsafe side. In the serviceability limit state, this issue is inversed. However, a realistic description of the deformation cannot be depicted. A bilinear curve considering the slip and the closed MVK would be more suitable. It is assumed that this increases the computational effort for complex models beyond a reasonable level.

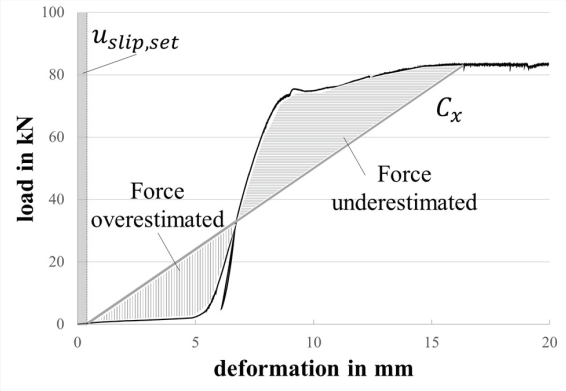

Figure 14: *Gradient of C_x from test series B and one load-deformation curve of a specimen of test series B*

The stiffness values are compared on the mean level, since no other regulations are specified for this purpose. [11]
Properties that could be applied from [11] are the distribution functions for the load-bearing capacity $R_{c,0}$ and $R_{c,90}$. However, these distribution functions differ in their nature. Thus, $R_{c,0}$ is defined as lognormally and $R_{c,90}$ as normally distributed. In order to be able to give a statement about this, an increase in the number of samples is necessary. Current evaluations show an inclination to the lognormal distributed function. This assumption has not yet been statistically tested.

5.2 VERIFICATION OF THE LOAD-BEARING BEHAVIOUR

The elastic results $R_{max,el,mean}$ are in the range of the results published in [8]. Due to the fact that the failure of the MVK is generated by the deformation of the front-notch, the values for the ultimate limit state must be defined at a set deformation limit. This may not represent the maximum elastic limit $R_{max,el,mean}$, which is given in section 4.1. It can be expected that the characteristic values will then approach the state of art for compression $F_{dim,compression}$.

Due to the experimental setup, only few results could be archived at loads above the elastic limit. Most of the tests had to be aborted because the specimen touched the testing frame or the loadcell was tilted. Therefore, only little reliable information about the plastic behavior was gained and no results can be presented.

5.3 VERIFICATION OF THE NODE STIFFNESS

The assumptions in the literature [16] for the stiffness of step joints, mainly rely on historical studies.

Different types of models of the displacement springs are used. In [17] the stiffness is given in two directions: parallel and perpendicular to the fibre – shown below for the MVK at the continuous lamella:

$$C_{\parallel} \approx C_{\perp} \approx 1 \cdot 10^5\ N/mm$$

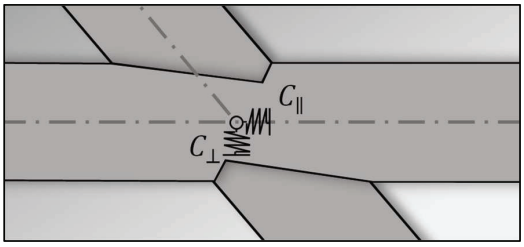

Figure 15: *Arrangement of the deformation springs in adaptation to the MVK*

This value significantly exceeds the resulting values for the MVK obtained in the current study. Another source [18] describes that the step joint can primarily transmit normal forces. This means that an elastic spring should be applied in the direction of the abutting lamella [19]. As a result, the node is designed to be hinged.

Forces perpendicular to the lamella only have a minor influence on the global load transfer. This allows for a rigid modelling regarding the shear forces.
In the mentioned literature[18], a value of the following stiffness has been assumed:

$$C_x \approx 45\ kN/mm$$

This stiffness results from a deformation of 15 mm at the elastic maximum compressive force in the direction of the abutting lamella.
This assumption fits to the result values of the tests.
In [8], another formulation for the stiffness of a step joint, is given by the following equation:

$$C_x[kN/mm] = (45.2 - 42.1 \cdot sin^2\gamma) \cdot \frac{b}{12} \cdot 1 + \frac{t_v - 2.34}{2.34} \cdot 0.1 \quad (6)$$

where b and t_v have the dimension cm

For the dimensions of the tested MVK, the resulting value is:

$$C_x \approx 20\ kN/mm$$

This value is below the load-bearing capacity of the node stiffness of the MVK, which is approximately 50 kN/mm. One possible explanation for the different results is the fact that the wood anisotropy causes very significant scattering. Especially the values from the historical investigation can be affected, because the regulation for sorting, wood moisture and assembly were not strictly specified at that time. Furthermore, different methods of measuring can lead to varying values. Regardless of these aspects, it is also assumed that the connection is strongly influenced by the stiffness perpendicular to the grain which varies considerably. [20] Therefore, there are no provisions for the distribution functions.

6 CONCLUSIONS

During experiments at the TU Braunschweig the load bearing behaviour and capacity as well as the stiffness of the MVK was evaluated. If a load is applied, deformations are primarily observed at the front-notch and bottom-notch surfaces of the MVK. Therefore, the load

https://doi.org/10.52202/069179-0199

deformation curve shows an almost linear elastic area followed by a large plastic area. Multiple test series allowed for the evaluation of the MVK in a pre-deformed and a quasi-perfect state. It was observed that a gap between the lamellae decreases the stiffness significantly while also reducing the load carrying capacity. The difference between the stiffnesses of these pre-deformed nodes and quasi-perfect nodes has to be considered in design.

The determined stiffness values can serve as the basis for a design concept that takes the stiffness distribution into account when determining the internal forces. In the lack of precise knowledge or predominant scattering effects, conservative approaches are usually adopted. In the case of internal force distributions, this does not mean to "lower" the stiffness values, as these lead to an underestimation of the internal forces. Therefore, a method shall be developed, which allows for a safe estimation of internal forces in ULS. Regarding the SLS on the other hand, the slip occurring in some connections can have a major influence on the deformation behaviour and needs to be considered. Further investigations are planned to be conducted on a prototype building located in a testing facility in Leipzig.

One goal in the development of the MVK was to improve the long-term behaviour compared to the Zollinger system. This aspect needs further investigation. Especially considering the load redistribution after closing of the gaps observed in the MVK in proximity to segment joints.

Due to the limitations of the testing equipment, notably the maximum movement during which the specimen could freely deform, no systematic valuation of the plastic deformation capacity could be made. However, qualitatively big plastic deformations can be observed. In order to exploit the full potential of the MVK, the plastic deformation capacity should be taken into consideration and included in the determination of C_u.

The curvature of the structure and therefore the needed bending of the board results in recoil forces that must be absorbed by the staples. However, it can be assumed that these forces decrease over time, so does the resistance of the stapled connection. This needs further investigation.

ACKNOWLEDGEMENT

These investigations were only possible due to project funding from Fachagentur Nachwachsende Rohstoffe e. V. (FNR, project no. 2220HV003C, funding period 2020-2023). A great thank you is given to the FLEX Team of the HTWK Leipzig as well as to the company STRAB GmbH and J. Bengel for the support in the organization, the setting and the delivery of the test specimens.

REFERENCES

[1] Wallner B. et al.: Holz-Holz-Verbindungen. Institut für Holzbau und Holztechnologie Technische Universität Graz. holz.bau forschungs gmbh, 2014.

[2] Erler K.: Kuppeln und Bogendächer aus Holz. Von arabischen Kuppeln bis zum Zollinger-Dach. Fraunhofer IRB Verlag Stuttgart, 2013.

[3] Tutsch J. F.: Weitgespannte Lamellendächer der frühen Moderne. Konstruktionsgeschichte, Geometrie und Tragverhalten. Technische Universität München, 2020.

[4] Zimmermann F., Bairstow C.: Das Dach der Zukunft. Zollinger Lamellendächer der 20er Jahre. Konstruktion, Statik, Ästhetik, Verbreitung, Nachfolge, Beispiele in Bayern. Fachhochschule München, 2003.

[5] Zollinger F.: Raumabschließende, ebene oder gekrümmte Bauteile. Patent Nr. 387469.

[6] Stahr A. et al.: Der Mikroversatzknoten – eine innovative Holzverbindung. *bmH bauen mit Holz,* 3.2019:22-29, 2019.

[7] Stahr A. et al.: Brettrippendächer in elementierter Bauweise. *bmH bauen mit Holz,* 7-8.2019:20-27, 2019.

[8] Heimeshoff B., Köhler N.: Untersuchung über das Tragverhalten von zimmermannsmäßigen Holzverbindungen. Im Auftrag der Entwicklungsgemeinschaft Holzbau (EGH) in der Deutschen Gesellschaft für Holzforschung e. V. (DGfH). Lehrstuhl für Baukonstruktion und Holzbau. Technische Universität München, 1989.

[9] *Timber structures; joints made with mechanical fasteners; General principles for the determination of strength and deformation characteristics*. DIN EN 26891:1991. CEN, July 1991.

[10] *National Annex – Nationally determined parameters – Eurocode 5: Design of timber structures – Part 1-1: General – Common rules and rules for buildings*. DIN EN 1995-1-1/NA. CEN, August 2013.

[11] *JSCC probabilistic model code Part 3: Resistance models.* Joint Committee on Structural Safety. August, 2006.

[12] Loebjinski M.: Bewertung der Tragfähigkeit von Holzkonstruktionen beim Bauen im Bestand – Ein Beitrag zur substanzschonenden Erhaltung von bestehenden Gebäuden. Lehrstuhl für Stahl- und Holzbau. Brandenburgische Technische Universität Cottbus – Senftenberg, July 2021.

[13] Colling F.: Holzbau Grundlagen und Bemessung nach EC 5. Springer-Verlag GmbH Wiesbaden, 2021.

[14] *Timber structures – Calculation and verification of characteristic values.* DIN EN 14358:2016. CEN, November 2016.

[15] *Eurocode 5: Design of timber structures – Part 1-1: General – Common rules and rules for buildings.* DIN EN 1995-1-1:2004. CEN, December 2010.

[16] Görlacher R., Falk V. C., Eckert H.: Historische Holztragwerke – Untersuchen, Berechnen und Instandsetzen. In Wenzel F., Kleinmanns J., editor, *Sonderforschungsbereich 315 „Erhalten historisch bedeutsamer Bauwerke", Karlsruhe. Jahrbuch 1996,* pages 219-245. Ernst & Sohn, Berlin, Germany, 1999.

[17] Blaß H. J., Falk V. C., Görlacher R.: Statische Modellierung der Nachgiebigkeiten historischer

Holzverbindungen. In Wenzel F., Kleinmanns J., editor, *Sonderforschungsbereich 315 „Erhalten historisch bedeutsamer Bauwerke“, Karlsruhe. Jahrbuch 1996,* pages 219-245. Ernst & Sohn, Berlin, Germany, 1999.

[18] Holzer S. M.: Statische Beurteilung historischer Tragwerke Band 2 Holzkonstruktionen. Ernst & Sohn Verlag, Berlin, 2016.

[19] Palma P., Cruz H.: Mechanical behaviour of traditional timber carpentry joints in service conditions – results of monotonic tests. In: From material to structure: Mechanical behaviour of the timber structures, Online Proceedings, 14.ICOMOS IWC Kolloquium, 2007.

[20] Kollmann F.: Technologie des Holzes und der Holzwerkstoffe Erster Band Anatomie und Pathologie, Chemie, Physik, Elastizität und Festigkeit. Springer-Verlag Berlin Heidelberg GmbH, 1951.

https://doi.org/10.52202/069179-0199